SCIENTIFIC REPORTS

OPEN

SUBJECT AREAS:
CATALYSIS
POLLUTION REMEDIATION

Received
25 July 2014

Accepted
7 October 2014

Published
28 October 2014

Correspondence and requests for materials should be addressed to Q.W. (qiang.wang.ox@gmail.com; qiangwang@bjfu.edu.cn)

Novel $Na_2Mo_4O_{13}$/α-MoO_3 hybrid material as highly efficient CWAO catalyst for dye degradation at ambient conditions

Zhang Zhang[1], Ruoyan Yang[1], Yanshan Gao[1], Yufei Zhao[2], Junyang Wang[1], Liang Huang[1], Jiang Guo[3], Tuantuan Zhou[1], Peng Lu[1], Zhanhu Guo[3] & Qiang Wang[1]

[1]College of Environmental Science and Engineering, Beijing Forestry University, 35 Qinghua East Road, Haidian District, Beijing 100083, P. R. China, [2]Key Laboratory of Photochemical Conversion and Optoelectronic Materials, Technical Institute of Physics and Chemistry, Chinese Academy of Sciences, Beijing, 100190, P. R. China, [3]Integrated Composites Laboratory, Dan F Smith Department of Chemical Engineering, Lamar University, Beaumont, TX 77710, USA.

We report a novel hybrid material $Na_2Mo_4O_{13}$/α-MoO_3 as highly efficient catalytic wet air oxidation (CWAO) catalyst, which showed the highest ever activity at room temperature and atmosphere pressure for the degradation of cationic red GTL. SEM and TEM analyses indicated that this hybrid catalyst has bamboo-shaped nanofiber morphology. In view of practical applications, the influence of some key parameters including operation temperature, catalyst calcination temperature, and the volume of dye wastewater have been optimized. The mechanism for the superior catalytic performance was investigated. XRD, XPS, and ESR suggested the $Na_2Mo_4O_{13}$/α-MoO_3 hybrid catalyst possesses more O^{2-} ions in the oxygen deficient regions than neat α-MoO_3, promoting the formation of active ·OH radicals and resulting in a higher activity. Considering the facile preparation and its superior activity, this novel catalyst is promising for practical dye wastewater treatment.

The dye wastewater generated from textile industries contains a wide variety of organic pollutants, which have a severe influence on both environment and human health. Even small amount of dyes in water (about 10–20 mg/L) is highly visible, affecting the water transparency and gas solubility, and consequently the photosynthetic activity in aquatic biota[1,2]. Some dyes can be considered as carcinogens or mutagens as well[3]. Therefore, it is urgent to search for a suitable method for the treatment of dye wastewater. Previously, many technologies have been developed, which include biological treatment[4], wet air oxidation (WAO)[5], ozone treatment[6], and chemical coagulation[7], etc. However, all the above methods have their own shortages[8–11]. For instance, although WAO method is very effective in removing color and chemical oxygen demand (COD), high temperature and pressure are always needed (e.g. 175–320°C, 0.5–20 MPa)[12–14]. Recent studies have proven that catalytic wet air oxidation (CWAO) is a very promising advanced oxidation process to efficiently degrade the dyes under relatively mild conditions[12]. Although CWAO can significantly relax the oxidation condition, it still requires a temperature in the range of 80–180°C and a pressure in the range of 1–5 MPa[15–17]. From the economical point of view, there is still a need and challenge to further improve the catalytic activity and the long-term stability of catalysts in order to achieve a more efficient degradation of organic compounds under a more mild condition. Particularly it will be ideal for practical applications if the dye wastewater can be efficiently treated at room temperature and atmosphere pressure.

For CWAO, the degradation activities of dyes are highly dependent on the catalysts used. Although there are many catalysts that have been reported for CWAO, only few of them can achieve high performances under room temperature and atmosphere pressure conditions. Such catalysts reported in literatures include Ce/MoO_3[17], $Zn_{1.5}PW_{12}O_{40}$[18], Mo-Zn-Al-O[19], ZnO/MoO_3/SiO_2[1], ZnO/MoO_3[20], CuO-MoO_3-P_2O_5[3], FeO_x-MoO_3-P_2O_5[3], Fe_2O_3-CeO_2-TiO_2/γ-Al_2O_3[21], $Zn_{1.5}PMo_{12}O_{40}$[22], etc. All these catalysts, their testing conditions, and catalytic performances were summarized in Table 1. The first CWAO catalyst (Fe_2O_3-CeO_2-TiO_2/γ-Al_2O_3) that showed high activity at room temperature and atmosphere pressure was reported by Liu and Sun in 2007[21]. With 100 mL and 500 mg/L methyl orange dye solution, 98.1% of color and 96.1% of total organic carbon (TOC) were removed

Table 1 | Summary of results from CWAO studies on the degradation of organic dyes

Catalysts	Catalyst amount (g)	Volume (mL)	Dye concentration (mg/L)	Testing temperature (°C)	Time (min)	$g_{catalyst}/g_{dye}$*	Adsorption rate (%)	Ref.
$Na_2Mo_4O_{13}/\alpha$-MoO_3	0.05	300	200	30	30	0.83	100.0	This work
Ce/MoO_3	0.1	100	300	25	20	3.3	98.0	17
$Zn_{1.5}PW_{12}O_{40}$	0.2	200	34.1	RT	360	29.3	80.0	18
Mo-Zn-Al-O	0.272	100	85	RT	60	32	80.1	19
$ZnO/MoO_3/SiO_2$	1	100	300	RT	25	33.3	95.3	1
ZnO/MoO_3	1	100	300	RT	18	33.3	98.0	20
CuO-MoO_3-P_2O_5	1.33	100	300	35	10	44.3	99.3	3
FeO_x-MoO_3-P_2O_5	1.33	100	300	35	30	44.3	98.0	25
Fe_2O_3-CeO_2-TiO_2/γ-Al_2O_3	3	100	500	25	150	60	98.1	21
$Zn_{1.5}PMo_{12}O_{40}$	0.1	100	10	RT	40	100	98.0	22

*$g_{catalyst}/g_{dye}$ represents the catalytic activity of catalysts, the lower value shows the higher catalytic activity of catalyst.

within 2.5 h at 25°C and 1 bar. However, a big amount of catalyst (3 g) was required, corresponding to a catalyst/dye ratio of 60. In the same year, Ma et al.[3] reported CuO-MoO_3-P_2O_5 and FeO_x-MoO_3-P_2O_5 catalysts that can achieve 98.0–99.3% color removal within 10 min (1.33 g catalyst, 100 mL, 300 mg/L, 35°C and 1 bar). The catalyst/dye ratio was slightly decreased, but still as high as 44.3. Later on, several more active catalysts such as ZnO/MoO_3[20], $ZnO/MoO_3/SiO_2$[1], Mo-Zn-Al-O[19], and $Zn_{1.5}PW_{12}O_{40}$[22] were developed, with the catalyst/dye ratio being decreased to 33.3, 33.3, 32, and 29.3, respectively. Up to date, the most active catalyst was Ce/MoO_3 with a catalyst/dye ratio of only 3.3. Under the testing condition of 0.1 g catalyst, 100 mL, and 300 mg/L Safranin-T, 98% degradation ratio could be achieved within 20 min at 25°C and 1 bar. In this contribution, we reported a new CWAO catalyst, $Na_2Mo_4O_{13}/\alpha$-MoO_3 hybrid material with remarkably higher catalytic activity at room temperature and atmosphere pressure. By adding only 0.05 g catalyst into 300 mL, 200 mg/L dye solution, a 100% decolorization rate could be reached within 30 min at 30°C and 1 bar. The catalyst/dye rate is only 0.83, the lowest value ever comparing to all the reported catalysts, suggesting that this new catalyst is highly feasible and promising for practical applications in dye wastewater treatments.

Results

A series of catalysts were first synthesized using hydrothermal method at 120°C with ammonium heptamolybdate tetrahydrate ($(NH_4)_6Mo_7O_{24}\cdot 4H_2O$) as precursor. The pH was controlled in the range of 1–7 by adding either HNO_3 or NaOH solution. We found that white products could be obtained when the pH was not higher than 6. However, no solid product was observed with a further increase in pH to 7. Then all the white products were calcined at 400°C in air for 5 h, and evaluated for the degradation of cationic red GTL, as shown in Figure 1. The results indicated that the synthesis pH had a great effect on the performance of obtained catalysts. Generally the activity of the catalysts increased with increasing the synthesis pH. When the synthesis pH was low (1–4), the catalytic activity was very poor, with a degradation efficiency lower than 40% after 90 min. When the synthesis pH was 5, the activity was significantly increased, with a degradation efficiency of ca. 80% after 90 min. But its activity was still not acceptable due to its relatively low kinetics. After 30 min, its degradation efficiency was only ca. 38%. However, surprisingly the catalyst synthesized at pH = 6 was observed to exhibit extremely high activity, i.e., 100% degradation efficiency was achieved within 35 min. This is the highest activity among all the reported CWAO catalysts when evaluated at room temperature and atmosphere pressure, with a catalyst/dye ratio of 1.67. Since for all the catalysts, the only difference was the synthesis pH, we are very much interested in how the synthesis pH influences the chemical composition and activity of the obtained catalysts. Thus, a thorough characterization of all the catalysts was performed in the following sections.

In order to have a better understanding of all the synthesized catalysts and make it clear what is the key parameter determining the activities, XRD analyses were carried out with both fresh and calcined samples. Figure 2(a) shows that when the pH = 1, pure h-MoO_3 was synthesized (JCPDS no. 21-0569)[23]. When the pH = 2, it favored the formation of hybrid compound containing $(NH_4)_2Mo_4O_{13}$ and $(NH_4)_4Mo_8O_{26}$. However, when the pH was in the range of 3–5, the diffraction peaks of $(NH_4)_4Mo_8O_{26}$ disappeared, suggesting the formation of pure $(NH_4)_2Mo_4O_{13}$. Further increasing the pH value to 6, a new hydrate compound of $NaNH_4Mo_3O_{10}\cdot H_2O$ was obtained. Figure 2(b) indicates that after the samples were calcined at 400°C, all the samples synthesized with pH in the range from 1 to 5 were transformed to pure α-MoO_3 (JCPDS No. 35-0609)[23]. The characteristic diffraction peaks of α-MoO_3 at 2θ = 12.78°, 23.34°, 25.70°, 27.34°, 33.76°, 38.98°, 46.32°, 49.26° and 58.8° can be indexed to the reflections of 020, 110, 040, 021, 111, 060, 061, 002 and 081, respectively. While the sample synthesized with pH = 6 was transformed into a hybrid material containing $Na_2Mo_4O_{13}$ and α-MoO_3. The characteristic peaks of $Na_2Mo_4O_{13}$ was observed at 2θ = 15.96°, 22.55°, 24.10°, 28.49°, 29.96°, and 32.41° (JCPDS No. 28-1112). Similar phenomenon had been previously observed by Sotani et al.[24] By thermal decomposing one type of hydrated potassium brone $K_{0.23}MoO_3(H_2O)_{0.43}$, similar

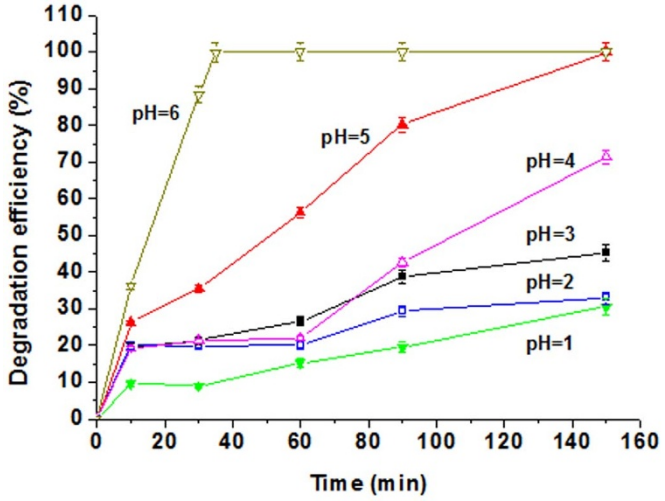

Figure 1 | The catalytic activity of catalysts synthesized at different pH ranging from 1 to 6. Test condition: 0.1 g catalyst (calcined at 400°C), 300 mL, 200 mg/L, 30°C, 1 bar.

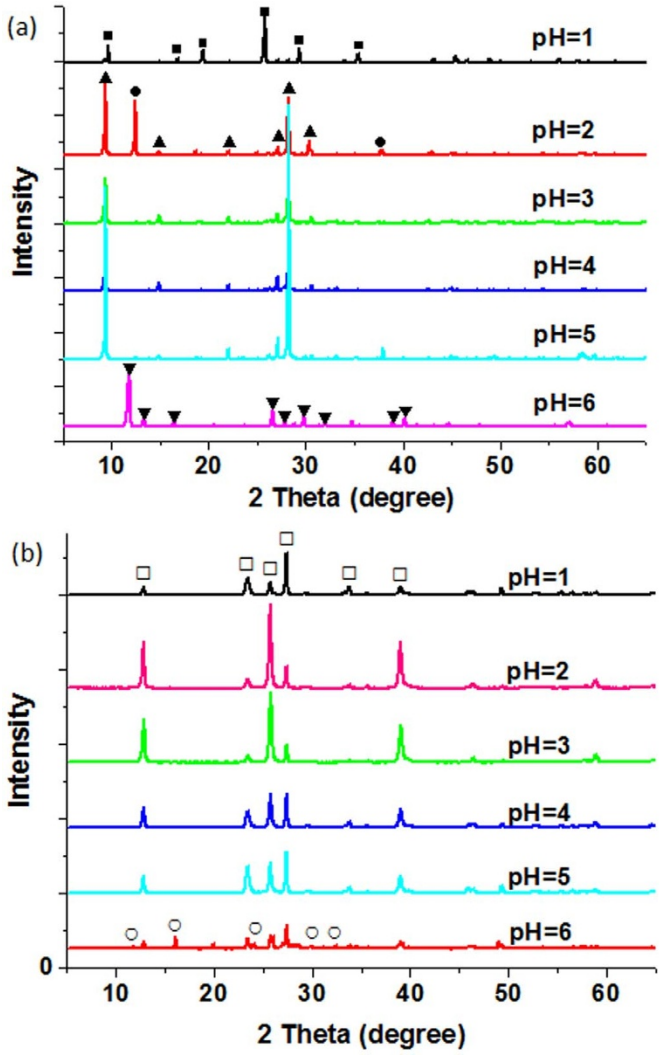

Figure 2 | XRD patterns of the samples synthesized with different pH. (a) before calcination, (b) after calcination at 400°C, (■) h-MoO_3, (▲) $(NH_4)_2Mo_4O_{13}$, (●) $(NH_4)_4Mo_8O_{26}$, (▼) $NaNH_4Mo_3O_{10}{\cdot}H_2O$, (□) α-$MoO_3$, and (○) $Na_2Mo_4O_{13}$.

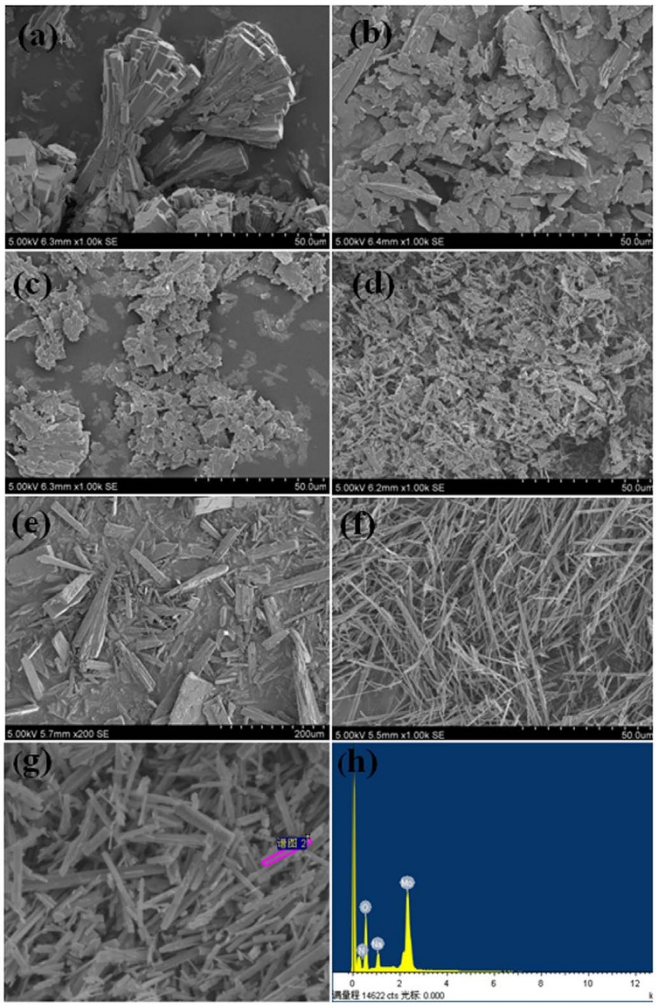

Figure 3 | SEM images of the samples prepared with a pH value of (a) 1, (b) 2, (c) 3, (d) 4, (e) 5, and (f) 6, and SEM-EDX analysis of the samples synthesized with pH = 6 (g and h) (before calcination).

hybrid materials consisting $K_2Mo_4O_{13}$ and MoO_3 were prepared[24]. In couple with the activity tests, these data clearly suggest that the catalytic activity of pure α-MoO_3 is moderate, consistent with the literature reports[1,3,17,20,25]. However, in the presence of $Na_2Mo_4O_{13}$, the activity was markedly improved, indicating that $Na_2Mo_4O_{13}$ plays a crucial role in this catalytic degradation of cationic red GTL reaction.

The samples were further characterized by FE-SEM and SEM-EDX. Figure 3 shows the typical SEM images that give a panoramic picture of all the fresh samples synthesized at different pH. Through the hydrothermal decomposition of precursor at pH = 1, well-defined h-MoO_3 nanorods were obtained. Figure 3(a) depicts a cluster of unique flower-like morphology of h-MoO_3 nanorods. With increasing the pH from 1 to 3, the morphology of the samples changed from nanorods to nanoplates (Figure 3(b,c)). With a further increase of pH from 3 to 5, the nanoplates were gradually cracked down into small pieces, transforming from nanoplates into nanofibers. At pH = 6, the sample was completely transformed into uniform nanofibers, with a chemical composition of $NaNH_4Mo_3O_{10}H_2O$ (Figure 3(f)). The energy dispersive X-ray spectroscopy analysis (EDX) was also analyzed with the fresh sample synthesized at pH = 6 (Figure 3(g,h)). Both Na and N elements were detected with a molar ratio of 1 : 1. Together with the XRD analysis, it further confirms the formation of $NaNH_4Mo_3O_{10}{\cdot}H_2O$ single crystals at pH = 6. It can be concluded that the synthesis pH value has an important effect on the morphology and size of the samples. Figure 4 illustrates that the morphology of catalysts was changed obviously after being calcined at 400°C. Although most of the samples maintained their overall morphologies, the previously well crystallized single crystals were cracked down into small pieces of nanoparticles due to the thermal decomposition. For instance, for the most active hybrid catalyst, i.e., $Na_2Mo_4O_{13}$/α-MoO_3, it was obtained by the thermal decomposition of $NaNH_4Mo_3O_{10}H_2O$ single crystal nanofibers. After being calcined at 400°C, it showed bamboo shaped nanofibers, which are composed of many nanoparticles connected together.

Figure 5 shows the TEM images and the SAED patterns of the hybrid catalyst $Na_2Mo_4O_{13}$/α-MoO_3. Figure 5(a) further confirms the bamboo like nanofiber morphology of the synthesized $Na_2Mo_4O_{13}$/α-MoO_3 catalyst, with a diameter of ca. 350–450 nm. HR-TEM analysis suggested that the major component of the nanofibers is α-MoO_3. The lattice spacing along two different directions can be observed in Figure 5(b), which correspond to d_{100} (3.6 nm) and d_{001} (3.9 nm) of the orthorhombic α-MoO_3 phase, respectively[26–28]. The SAED pattern (Figure 5(d)) of the sample in Figure 5(c) also confirms the formation of α-MoO_3 phase, with the [-1-10] direction as the zone axis[26,29]. In addition, how the

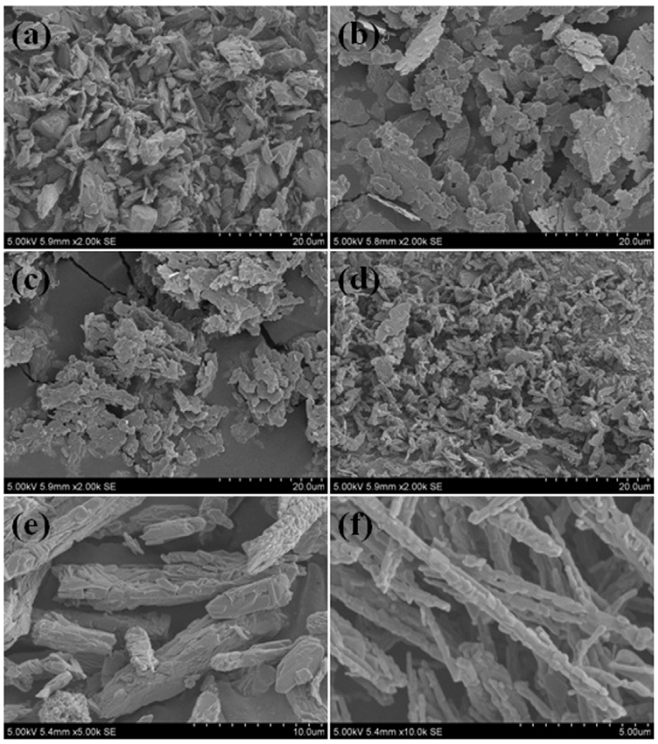

Figure 4 | **SEM images of the samples prepared with a pH value of (a) 1, (b) 2, (c) 3, (d) 4, (e) 5, and (f) 6 (after calcination).**

$Na_2Mo_4O_{13}$ phase is distributed within the sample is more interesting. During the thermal transformation process from the $NaNH_4Mo_3O_{10}{\cdot}H_2O$ single crystals to the hybrid material $Na_2Mo_4O_{13}$/α-MoO_3, since the calcination temperature (300–400°C) was not too high, we can expect that the $Na_2Mo_4O_{13}$ must disperse well with limited agglomerations. Thus, elemental mappings with Mo, O, and Na, Figure 5(e–h), clearly indicate that the Na element was distributed uniformly within the sample. This data suggests that the particle size of $Na_2Mo_4O_{13}$ should be very small and it was uniformly distributed within the α-MoO_3 phase. Both the existence of nano-phased $Na_2Mo_4O_{13}$ and the abundant interfaces created between $Na_2Mo_4O_{13}$ and α-MoO_3 are believed to play an important role in its superior catalytic activity.

By now, novel hybrid materials $Na_2Mo_4O_{13}$/α-MoO_3 with bamboo shaped nanofiber morphology have been demonstrated as a highly efficient catalyst for the degradation of cationic red GTL. However, for its practical applications, several important parameters have to be optimized, such as the operation temperature, catalyst calcination temperature, and the volume of dye wastewater, etc. Since this catalyst is aimed to treat dyes at ambient conditions, three temperatures of 25, 30, and 35°C were chosen. Figure 6(a) depicts the influence of testing temperatures on the degradation efficiency. It is obvious that the catalytic performance of catalyst was changed significantly as varying the testing temperature. Higher temperature resulted in higher degradation efficiency. At 25°C, it took 60 min to reach 100% degradation efficiency. While only 35 and 17 min were needed at 30 and 35°C, respectively. This data suggests that the operation temperature is one of the key parameters and has a great influence on the catalytic activity of the hybrid catalyst $Na_2Mo_4O_{13}$/α-MoO_3. Considering that the activity at 25°C is too low and the temperature of dye wastewaters is rarely as high as 35°C, all the following tests were performed at 30°C.

In addition, in order to demonstrate that the removal of cationic red GTL from wastewater is truly due to the catalytic oxidation, not adsorption, an adsorption experiment was designed and carried out as well. To prevent the influence of O_2 dissolved in H_2O, the dye

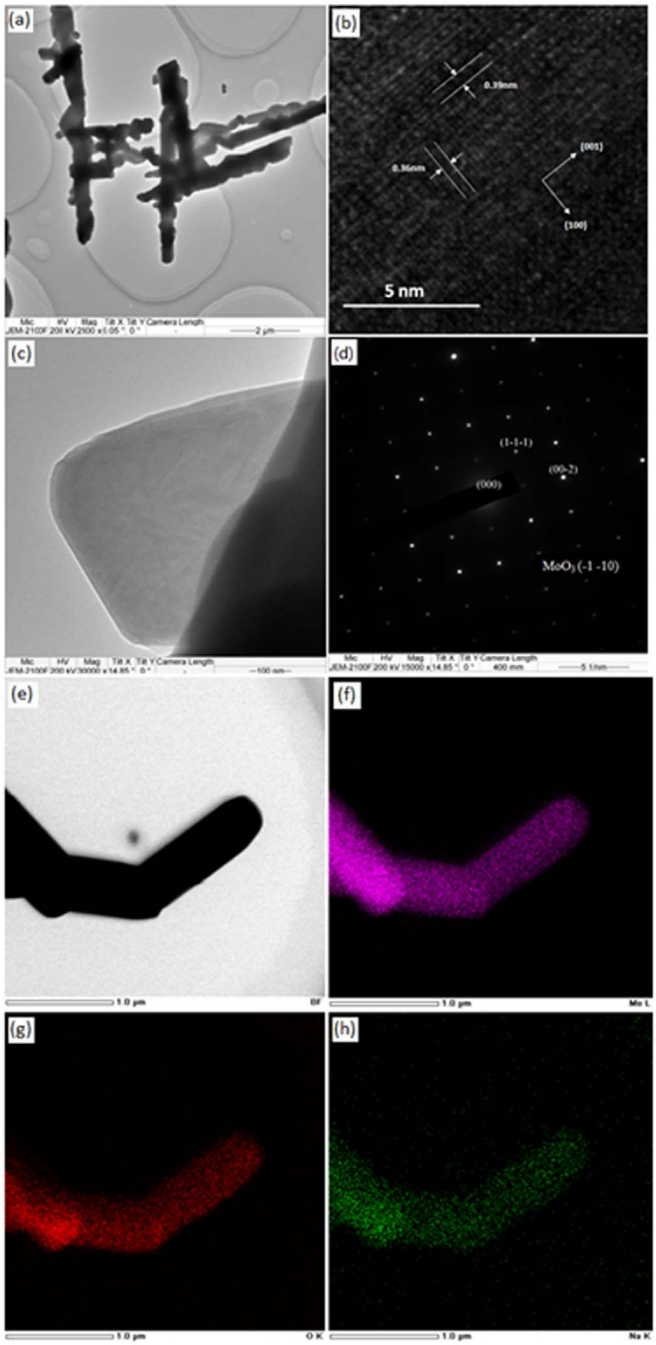

Figure 5 | (a–c) HR-TEM images and (d) SAED patterns of the synthesized $Na_2Mo_4O_{13}$/α-MoO_3 hybrid catalyst. (e) TEM image, and elemental (f) Mo mapping, (g) O mapping, and (h) Na mapping of the synthesized $Na_2Mo_4O_{13}$/α-MoO_3 hybrid catalyst.

solution was first purged with N_2 for at least 30 min before adding the catalyst. And during the whole test, the system was protected with continuous N_2, by which the catalytic oxidation of dyes can be ignored. As shown in Figure 6(a), the adsorption of cationic red GTL was very low, with a removal rate of only 22.8% after 150 min. This experiment clearly indicated that the adsorption of cationic red GTL by catalyst was not obvious and the true activity came from the catalytic oxidation in the presence of O_2.

It is well accepted that the calcination temperature might influence the decomposition process, which in turn determine the composition and phase of the obtained catalysts. The influence of calcination temperatures on this novel catalyst $Na_2Mo_4O_{13}$/α-MoO_3 was

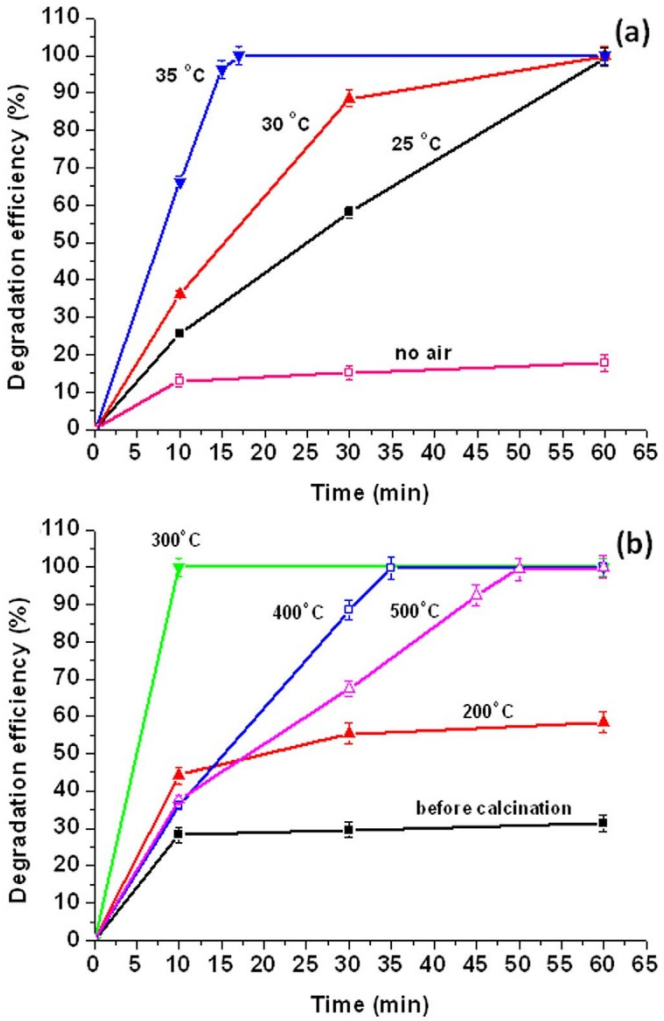

Figure 6 | (a) The influence of testing temperatures and O_2 on the degradation efficiency of cationic red GTL. (b) The influence of calcination temperature on the degradation efficiency of cationic red GTL. Testing condition: 0.1 g catalyst, 300 mL, 200 mg/L, 30°C, 1 bar.

studied. Figure 6(b) shows that its activity was very low with only 31.37% degradation efficiency after 60 min for the catalyst without any thermal treatment. However, the activities could be significantly improved after being calacined at 200–500°C. With increasing the calcination temperature, the activity of catalyst was first increased in the range from room temperature to 300°C, then started to decrease in the range from 300 to 500°C. The best calcination temperature was found to be 300°C, the obtained catalyst demonstrated a 100% of dyes being degraded within only 10 min. Thus, it can be concluded that the calcination temperature also has a great effect on the activity of the novel hybrid catalyst $Na_2Mo_4O_{13}$/α-MoO_3 and the optimal calcination temperature is 300°C.

With a fixed dosage of catalyst, how much wastewater can be processed is another important parameter for practical application. Apparently the more wastewater the catalyst can treat, the more economical and feasible it will be. Thus, the influence of wastewater volume in the range of 300–500 mL was evaluated with 0.1 and 0.05 g catalyst, respectively. The dye concentration was fixed at 200 mg/L. Figure S1 indicates that the degradation efficiency gradually was decreased with increasing the wastewater volume. The higher the volume was, the longer the time was needed for the 100% degradation efficiency. With 0.1 g catalyst, all three volumes reached 100% degradation within 30 min, particularly when the wastewater volume was 300 mL, only 10 min was needed. When the catalyst was reduced to 0.05 g, a relatively longer time was needed for 100% degradation, for instance, 30, 60, and 150 min for 300, 400, and 500 mL, respectively. Since a longer reaction time will increase the energy penalty, 0.05 g catalyst was recommended for usage to treat 300 mL wastewater, in which all dyes could be completely degraded within 30 min.

To further evaluate the catalytic activity of $Na_2Mo_4O_{13}$/α-MoO_3 hybrid catalyst, mineralization of cationic red GTL was investigated by monitoring the changes of TOC as a function of reaction time. Figure S2(a) indicates that the $Na_2Mo_4O_{13}$/α-MoO_3 hybrid catalyst is very active, a TOC removal rate of ca. 93% was achieved within 5 min. The long-term stability of the catalyst is extremely essential for its practical application. Figure S2(b) shows the degradation efficiency of cationic red GTL in the presence of $Na_2Mo_4O_{13}$/α-MoO_3 hybrid catalyst during the cycling tests. The catalyst exhibited a very good durability and there was almost no noticeable decrease in the activity even after seven cycles. The degradation percentage of cationic red GTL still reached a value of 99.53% even after 7th cycle.

Discussions

In order to know whether the containing of Na is the key parameter determining the catalytic activity, we conducted a control experiment that a series of samples were synthesized at different pH by adding certain amount of $NaNO_3$ (2.04 g) during each synthesis. XRD analyses were carried out with both fresh and calcined samples. As shown in Figure 7(a) that when the pH = 1, pure $(NH_4)_4Mo_8O_{26}$ was synthesized. With the synthesis pH increased from 2 to 3, we found the existence of a kind of hybrid compound which contains $(NH_4)_4Mo_8O_{26}$ and $(NH_4)_2Mo_4O_{13}$. When the pH value was in the range of 4–6, the diffraction peaks of $(NH_4)_4Mo_8O_{26}$ were disappeared, and a new compound of $NaNH_4Mo_3O_{10}{\cdot}H_2O$ was synthesized at the same time. Figure 7(b) indicates that after the calcination at 400°C for 5 h, all samples synthesized with pH in the range from 1 to 3 transformed into pure α-MoO_3. However, when the synthesis pH = 4−6, the sample transferred into α-MoO_3/$Na_2Mo_4O_{13}$ hybrid materials.

As the XRD analyses had confirmed the formation of the new hybrid material of $Na_2Mo_4O_{13}$/α-MoO_3, we performed a further study to verify the high catalytic activity of this novel hybrid material. It can be seen from Figure 8 that the catalytic activity of catalysts also increased with the increase in synthesis pH. Under the same test condition, the catalytic activity of samples which were synthesized at lower pH value (pH=1 and 2) was very poor, with the degradation efficiency of 23.55% and 49.71%, respectively. However, when the synthesis pH increased to 3, the activity significantly increased with nearly 100% removal of dye after 90 min. While when the synthesis pH was increased to 4−6, we found that all catalysts showed high catalytic activity, 100% of degradation efficiency can be reached within 30 min. It can be concluded that the novel $Na_2Mo_4O_{13}$/α-MoO_3 hybrid material can be synthesized at relatively lower pH when $NaNO_3$ was added in the synthesis. It also demonstrated that Na plays an important role in the formation of this kind of hybrid material. And the degradation test of this series of new samples confirmed the high activity of $Na_2Mo_4O_{13}$/α-MoO_3 and the synthesis pH surely has effect on the catalytic activity.

The above data has shown that the calcination temperature has a great effect on its catalytic activity. In order to have a deep understanding of this phenomenon, the thermal decomposition process of the sample synthesized at pH = 6 was monitored using XRD analysis. Figure 9 shows the XRD patterns of the catalysts that being calcined at different temperatures (200–500°C). Before calcination, the sample synthesized at pH = 6 formed a single crystal of $NaNH_4Mo_3O_{10}{\cdot}H_2O$. After being calcined at 200°C, $NaNH_4Mo_3O_{10}{\cdot}H_2O$ started to be partially decomposed. As the calcination temperature increased to 300°C, the active hybrid catalyst

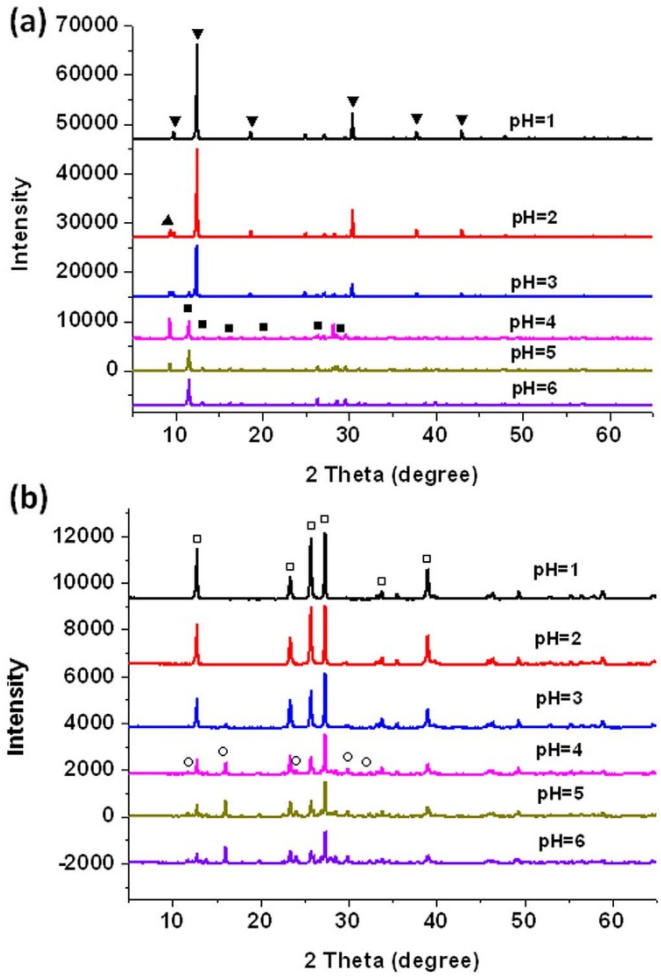

Figure 7 | XRD patterns of the samples synthesized with different pH and $NaNO_3$ added, (a) before calcination, (b) after calcination at 400°C, (▼) $(NH_4)_4Mo_8O_{26}$, (▲) $(NH_4)_2Mo_4O_{13}$, (■) $NaNH_4Mo_3O_{10}\cdot H_2O$, (□) α-$MoO_3$, and (○) $Na_2Mo_4O_{13}$.

containing $Na_2Mo_4O_{13}$ and α-MoO_3 was synthesized. The intensity of $Na_2Mo_4O_{13}$ in the hybrid catalyst was weakened at 400°C and disappeared at 500°C. This trend is consistent with the catalytic activity test, which first increased with the calcination temperature up to 300°C, and then started to decrease from 400 to 500°C. This data clearly suggests that the existence of $Na_2Mo_4O_{13}$ is critical for its good catalytic activity.

The catalytic degradation process of cationic red GTL was monitored using UV-Vis spectroscopy. Figure 10(a) shows the evolution of the UV-Vis spectra of the dye solution as a function of reaction time in the presence of $Na_2Mo_4O_{13}$/α-MoO_3 catalyst and bubbled air. At the initial stage, two major absorbance peaks at 285 and 488 nm were observed and attributed to the benzene ring and the azo linkage of cationic red GTL[30]. However, these two peaks were significantly weakened after 20 min, and completely disappeared after 30 min, indicating that the cationic red GTL molecules were destroyed by catalytic oxidation. The absorbance peak at 203 nm also became weaker in intensity and offset in the direction of long wavelength. After 30 min, a new absorbance peak at 213 nm appeared and its intensity increased with increasing the reaction time, suggesting the production of a new kind of intermediates during the reaction[31]. However, if N_2 instead of air was used, a totally different evolution of the UV-Vis spectra was observed, as shown in Figure 10(b). With increasing the treatment time, those three characteristic peaks at 203, 285, and 488 nm still remained, with a slight

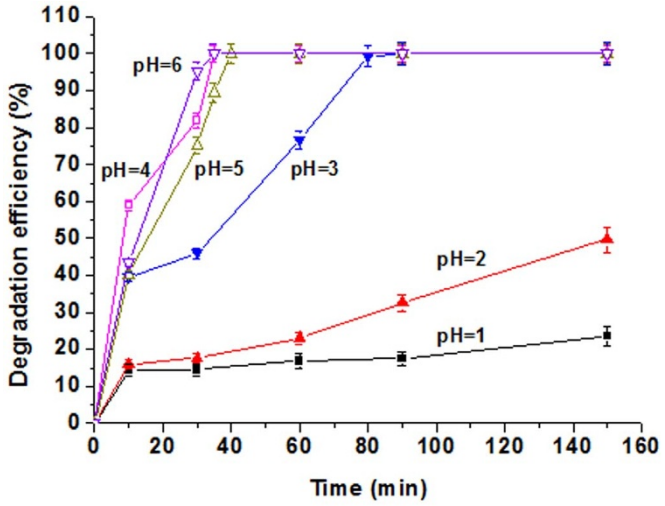

Figure 8 | The catalytic activity of catalysts synthesized at different pH ranging from 1 to 6 with $NaNO_3$ added. Test condition: 0.1 g catalyst (calcined at 400°C), 300 mL, 200 mg/L, 30°C, 1 bar.

decrease in intensity. This data further demonstrates that O_2 is critical for the catalytic degradation of dyes. In the absence of O_2, catalytic reaction can not be preceded due to the absence of active ·OH radical, and only a moderate adsorption occurred on the surface of catalyst[19]. The specific surface area of the sample synthesized at pH = 6 was also analyzed using N_2 adsorption-desorption isotherm. Before calcination, the product was $NaNH_4Mo_3O_{10}\cdot H_2O$ and its specific surface area was 1.0 m^2/g. After being calcined at 400°C, the product transformed into $Na_2Mo_4O_{13}$/α-MoO_3 and its specific surface area was 2.9 m^2/g. With such low specific surface area, it is reasonable that the adsorption of dye was negligible and the main function was catalytic oxidation.

Figure S3 shows the XPS survey spectra of α-MoO_3 and $Na_2Mo_4O_{13}$/α-MoO_3, both of which exhibit dominant peaks of Mo and O, along with a C 1s peak due to the surface contamination by sample handling or instrument background. In addition, an extra Na 1s peak was observed for $Na_2Mo_4O_{13}$/α-MoO_3 at 1070.9 eV. Figure 11(a,b) shows that the O1s peaks are asymmetric and broad, suggesting the coexistence of adsorbed oxygen with high binding energy and lattice oxygen with low binding energy on the surface of catalysts. The peak centered at 530 eV was associated with the

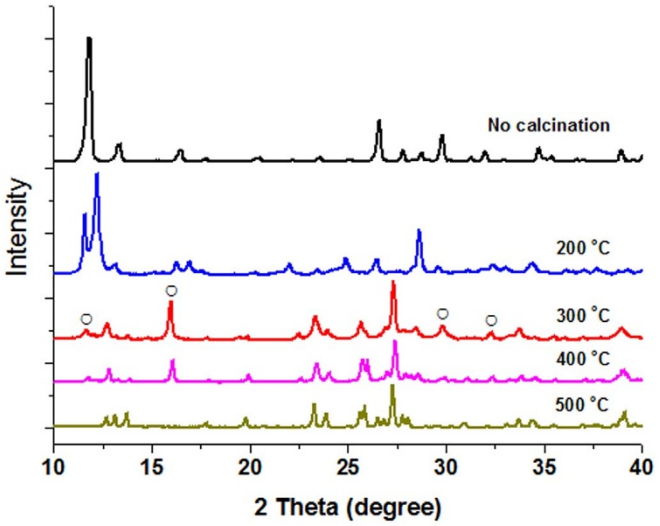

Figure 9 | XRD patterns of the catalyst calcined at different temperatures, (○) $Na_2Mo_4O_{13}$.

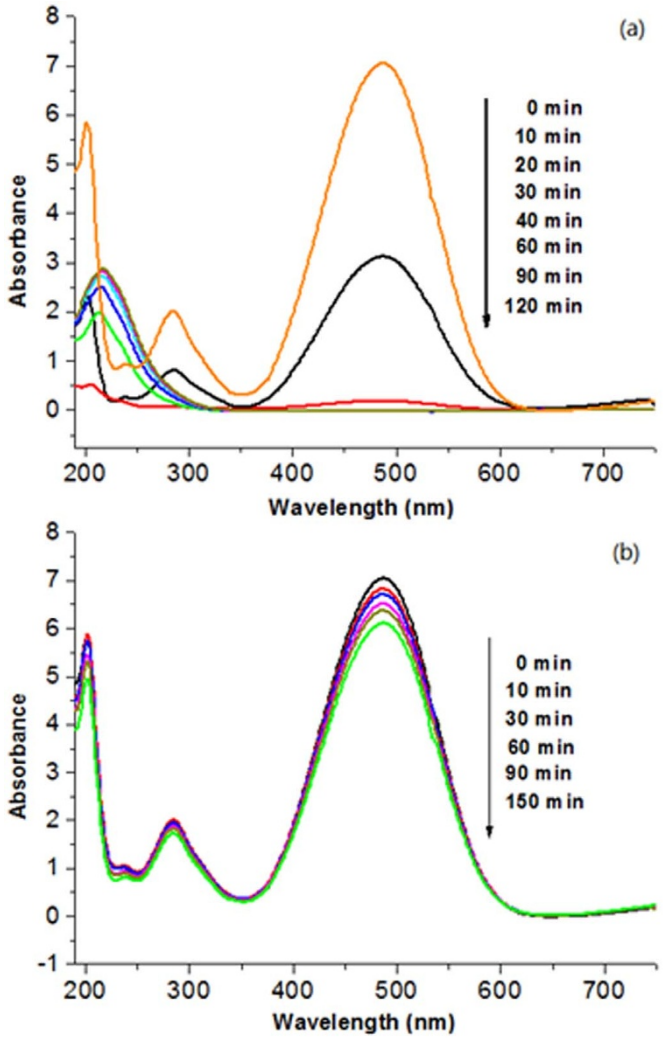

Figure 10 | The UV-Vis absorption spectral changes of the cationic red GTL solution as a function of (a) catalytic treatment time, and (b) adsorption time. Testing condition: 0.05 g catalyst (calcined at 400°C), 300 mL, 200 mg/L, 1 bar.

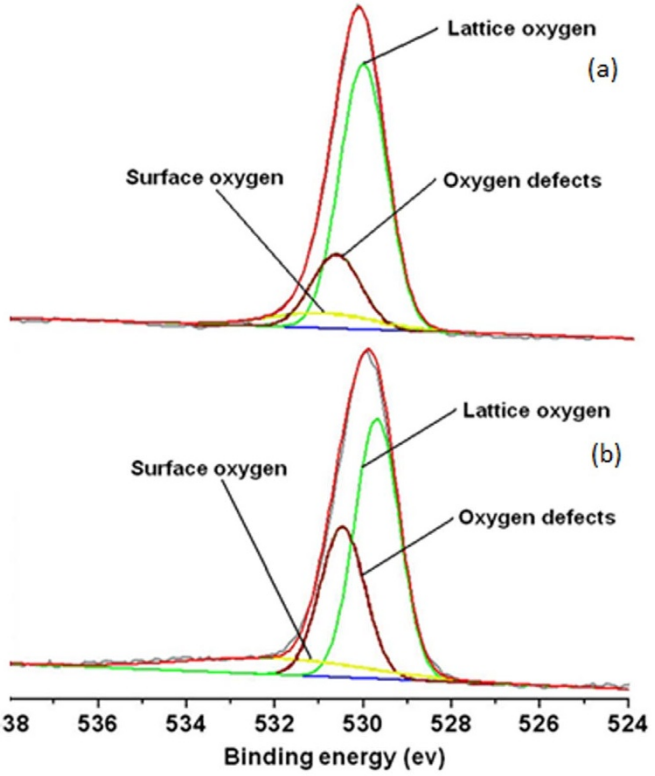

Figure 11 | O 1s spectra of (a) α-MoO_3, and (b) $Na_2Mo_4O_{13}$/α-MoO_3 hybrid catalysts.

O^{2-} ions in the metal oxide, the peak at 530.6 eV was associated with the O^{2-} ions in the oxygen deficient regions, and the binding energy peak at 530.9 eV was attributed to the surface loosely bound O_2[17]. Figure 11(a,b) clearly shows that the relative concentration of O^{2-} ions in the oxygen deficient regions for $Na_2Mo_4O_{13}$/α-MoO_3 is higher than that for α-MoO_3. This data suggests that more defects were created due to the coexistence of $Na_2Mo_4O_{13}$ and α-MoO_3 in the hybrid catalyst[32,33]. According to the literature, the O^{2-} ions in the oxygen deficient regions which have higher mobility than lattice oxygen, can actively take part in the oxidation process and greatly contribute to the catalyst activity[32,34].

Particularly, the higher concentration of the O^{2-} ions in the oxygen deficient regions in the $Na_2Mo_4O_{13}$/α-MoO_3 hybrid catalyst might promote the formation of active ·OH radicals. In order to prove this, ESR analysis was performed by placing both α-MoO_3 and $Na_2Mo_4O_{13}$/α-MoO_3 in water (Figure 12). When the solution was bubbled with air, four characteristic peaks of DMPO-·OH were clearly observed for both α-MoO_3 and $Na_2Mo_4O_{13}$/α-MoO_3 catalysts. And the ·OH intensity for $Na_2Mo_4O_{13}$/α-MoO_3 is higher than that for α-MoO_3, suggesting that more ·OH radicals were produced than α-MoO_3 under the same condition. It is also worth to mention that when the solution was bubbled with N_2, no ·OH signal was observed. This data provided the intrinsic reason why $Na_2Mo_4O_{13}$/α-MoO_3 is more active than α-MoO_3 and O_2 is essential for the catalytic oxidation reaction.

In conclusion, a novel hybrid CWAO catalyst of $Na_2Mo_4O_{13}$/α-MoO_3 was synthesized using a facile hydrothermal method and demonstrated extremely high catalytic activity for the degradation of cationic red GTL even at room temperature and atmosphere pressure, favorable for practical applications. With only 0.05 g catalyst, and 300 mL, 200 mg/L dye wastewater, 100% degradation efficiency could be achieved within 30 min at 30°C and 1 bar. Compared to all the reported catalysts in literature, it showed the highest activity ever, with a catalyst/dye ratio as low as 0.83. This new catalyst was thoroughly characterized and its operation parameters were optimized. Finally, the co-existence of $Na_2Mo_4O_{13}$ within the α-MoO_3 phase was demonstrated to be crucial, producing more interfaces and more O^{2-} ions in the oxygen deficient regions. It was believed that the O^{2-} ions in the oxygen deficient regions with higher mobility than lattice

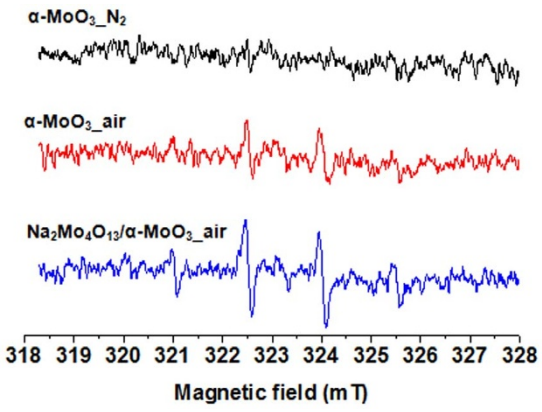

Figure 12 | ESR spectra of DMPO-·OH for α-MoO_3 and $Na_2Mo_4O_{13}$/α-MoO_3 in aqueous dispersions bubbled with air or N_2.

oxygen can promote the formation of ·OH radicals and actively take part in the catalytic oxidation reactions.

Methods

Synthesis of catalysts. The catalysts were synthesized using a hydrothermal route. Briefly, $(NH_4)_6Mo_7O_{24}{\cdot}4H_2O$ (26.48 g) was dissolved in 50 mL distilled water to form a clear solution at 50°C. HNO_3 or NaOH (4 M) solution was added dropwise into $(NH_4)_6Mo_7O_{24}{\cdot}4H_2O$ solution under magnetic stirring to control the pH value at 1–7. The resultant solution was transferred to a Teflon-lined stainless steel autoclave and heated at 120°C for 18 h. The produced precipitate was filtered and rinsed with deionized water and acetone, followed by drying at 60°C for 24 h. For the control experiment, the samples were synthesized at different pH using the same condition except that additional of 2.04 g $NaNO_3$ was added for each synthesis. After careful grinding, the as-prepared samples were calcined in air at certain temperatures (200–500°C) for 5 h with the heating rate of 10°C/min. The calcined samples were directly used as CWAO catalysts for the degradation of cationic red GTL.

Characterization of samples. X-ray diffraction (XRD) measurements of the catalyst powders were recorded using a Shimadzu XRD-7000 instrument in reflection mode with Cu Kα radiation. The accelerating voltage was set at 40 kV with 30 mA current ($\lambda = 1.542$ Å) at 0.1° s^{-1} from 5 to 65°. Field emission scanning electron microscopy (FE-SEM) and energy-dispersive X-ray spectroscopy (EDX) analyses were performed on a SU-8020 scanning electron microscope (SEM, HITACHI, Japan) with an accelerating voltage of 5.0 kV. Powder samples were spread on carbon tape adhered to SEM stage. Before observation, the samples were sputter coated with a thin platinum layer to prevent charging and to improve the image quality. High resolution transmission electron microscopy (HR-TEM), selected area electron diffraction patterns (SAED), and elemental mapping analysis were performed on JEM-2100 microscope (JEOL, Japan) with an accelerating voltage of 200 kV. Catalysts samples were dispersed in methanol with sonication and then cast onto copper grids coated with Formvar film. The BET specific surface areas (SSA) were measured from the N_2 adsorption and desorption isotherms at 77 K collected from an ASAP 2020 physisorption analyzer (Micromeritics). X-ray photoelectron spectroscopy (XPS) was carried out using a PHI Quantro SXM analyzer to analyze the chemical state of surface elements for the catalysts. The kinetic energies of photoelectrons were measured using a hemispherical electrostatic analyzer working in a constant pass energy mode. The C 1s peak from the adventitious carbon-based contaminant with a binding energy of 284.8 eV, was used as the reference for calibration. Electron spin resonance (ESR) signal of radicals was obtained on a JEOL FA-200 spectrometer that has been used to detect radical species by their unpaired electrons. The regent for the spin-trapping ·OH was T5,5-dimethyl-1-pyrroline-N-oxide (DMPO). For all the samples, the same quartz capillary tube was used to minimize experimental errors.

Catalytic activity tests. The CWAO tests were performed by adding certain amount of catalysts (0.05 or 0.1 g) into a simulated dye wastewater solution containing 200 mg/L cationic red GTL. The volume of the solution was changed in the range of 200–500 mL to evaluate the activity of catalysts under different catalyst/dye ratios. The experiments were conducted in a glass reactor with a capacity of 500 mL equipped with a magnetic stirrer. Air was injected into the bottom of the suspension with a flow rate of 0.4 L/min. About 3 mL samples were taken out by filtration at regular intervals. Visible light spectroscopy was used to monitor the degradation of cationic red GTL at a wavelength of 488 nm. UV-Visible spectra were performed using a using a UV 2600 UV-Vis spectrophotometer. TOC was monitored using a Shimadzu TOC-V CSN total organic carbon analysis system.

The durability was investigated by re-using the catalyst in a cycling test. The cycling runs were carried out by adding 0.1 g catalyst into a simulated dye wastewater solution containing 200 mg/L cationic red GTL. The volume of the solution was maintained 500 mL during all the runs. The experiments were conducted in a glass reactor with a capacity of 1000 mL equipped with a magnetic stirrer. Air was injected into the bottom of the suspension with a flow rate of 0.4 L/min. 10 mL samples were taken out by filtration every 30 minutes. In order to maintain the initial concentration of cationic red GTL, another 10 mL 10000 mg/L cationic red GTL solution was added into the reactor. Visible light spectroscopy was used to monitor the degradation of cationic red GTL at a wavelength of 488 nm. The cycles were repeated for 7 times.

1. Yuan, M., Wang, S., Wang, X., Zhao, L. & Hao, T. Removal of organic dye by air and macroporous $ZnO/MoO_3/SiO_2$ hybrid under room conditions. *Appl. Surf. Sci.* **257**, 7913 (2011).
2. Chung, K. T. & Stevens, S. E. Degradation of azo dyes by environmental microorganisms and helminthes. *Environ. Toxicol. Chem.* **12**, 2121 (1993).
3. Ma, H., Zhuo, Q. & Wang, B. Characteristics of $CuO\text{-}MoO_3\text{-}P_2O_5$ catalyst and its catalytic wet oxidation (CWO) of dye wastewater under extremely mild conditions. *Environ. Sci. Technol.* **41**, 7491 (2007).
4. Malachova, K., Rybkova, Z., Sezimova, H., Cerven, J. & Novotny, C. Biodegradation and detoxification potential of rotating biological contactor (RBC) with Irpex lacteus for remediation of dye-containing wastewater. *Water Res.* **47**, 7143 (2013).
5. Fox, M. & Noike, T. Wet oxidation pretreatment for the increase in anaerobic biodegradability of newspaper waste. *Bioresour. Technol.* **91**, 273 (2004).
6. Parsa, J. B. & Negandar, S. H. Treatment of wastewater containing Acid Blue 92 dye by advanced ozone-based oxidation methods. *Sep. Purif. Technol.* **98**, 315 (2012).
7. Lau, Y.-Y. *et al.* Coagulation-flocculation of azo dye Acid Orange 7 with green refined laterite soil. *Chem. Eng. J.* **246**, 383 (2014).
8. Alkaram, U. F., Mukhlis, A. A. & Al-Dujaili, A. H. The removal of phenol from aqueous solutions by adsorption using surfactant-modified bentonite and kaolinite. *J. Hazard. Mater.* **169**, 324 (2009).
9. Gupta, V. K., Ali, S. I. & Saini, V. K. Removal of rhodamine B, fast green, and methylene blue from wastewater using red mud, an aluminum industry waste. *Ind. Eng. Chem. Res.* **43**, 1740 (2004).
10. Vimonses, V., Jin, B. & Chow, C. W. K. Insight into removal kinetic and mechanisms of anionic dye by calcined clay materials and lime. *J. Membr. Sci.* **177**, 420 (2010).
11. Kansal, S. K., Singh, M. & Sud, D. J. Studies on photodegradation of two commercial dyes in aqueous phase using different photocatalysts. *J. Hazard. Mater.* **141**, 581 (2007).
12. Sonnen, D. M., Reiner, R. S. & Weinstock, I. A. Degradation of pulp-mill effluent by oxygen and $Na_5[PV_2Mo_{10}O_{40}]$, a multipurpose delignification and wet air oxidation catalyst. *Ind. Eng. Chem. Res.* **36**, 4134 (1998).
13. Neri, G., Pistone, A., Milone, C. & Galvagno, S. Wet air oxidation of p-coumaric acid over promoted ceria catalysts. *Appl. Catal. B: Environ.* **38**, 321 (2002).
14. Kim, S. C. & Lee, D. K. Preparation of Al–Cu pillared clay catalysts for the catalytic wet oxidation of reactive dyes. *Catal. Today* **97**, 153 (2004).
15. Lee, D. K. *et al.* Catalytic wet oxidation of reactive dyes with H_2/O_2 mixture on Pd–Pt/Al_2O_3 catalysts. *Sep. Purif. Technol.* **34**, 43 (2004).
16. Guo, J. & Al-Dahhan, M. Catalytic wet air oxidation of phenol in concurrent downflow and upflow packed-bed reactors over pillared clay catalysts. *Chem. Eng. Sci.* **60**, 735 (2005).
17. Li, W. *et al.* Fast catalytic degradation of organic dye with air and MoO_3:Ce nanofibers under room condition. *Appl. Catal. B: Environ.* **92**, 333 (2009).
18. Chai, F., Wang, L., Xu, L., Wang, X. & Huang, J. Degradation of dye on polyoxotungstate nanotube under molecular oxygen. *Dyes Pigm.* **76**, 113 (2008).
19. Xu, Y., Li, X. Y., Cheng, X., Sun, D. Z. & Wang, X. Y. Degradation of cationic red GTL by catalytic wet air oxidation over Mo-Zn-Al-O catalyst under room temperature and atmospheric pressure. *Environ. Sci. Technol.* **46**, 2856 (2012).
20. Huang, J., Wang, X., Li, S. & Wang, Y. ZnO/MoO_3 mixed oxide nanotube: A highly efficient and stable catalyst for degradation of dye by air under room conditions. *Appl. Surf. Sci.* **257**, 116 (2010).
21. Liu, Y. & Sun, D. Z. Development of $Fe_2O_3\text{-}CeO_2\text{-}TiO_2/\gamma\text{-}Al_2O_3$ as catalyst for catalytic wet air oxidation of methyl orange azo dye under room condition. *Appl. Catal. B: Environ.* **72**, 205 (2007).
22. Zhang, Y., Li, D., Chen, Y., Wang, X. & Wang, S. Catalytic wet air oxidation of dye pollutants by polyoxomolybdate nanotubes under room condition. *Appl. Catal. B: Environ.* **86**, 182 (2009).
23. Chithambararaj, A. & Bose, A. C. Hydrothermal synthesis of hexagonal and orthorhombic MoO_3 nanoparticles. *J. Alloys Compd.* **509**, 8105 (2011).
24. Sotani, N., Suzuki, T. & Eda, K. Preparation of hydrated potassium molybdenum bronzes and their thermal decomposition. *J. Solid State Chem.* **132**, 330 (1997).
25. Zhuo, Q., Ma, H., Wang, B. & Fan, F. Degradation of methylene blue: Optimization of operating condition through a statistical technique and environmental estimate of the treated wastewater. *J. Hazard. Mater.* **153**, 44 (2008).
26. Chen, Y. *et al.* Single-crystalline orthorhombic molybdenum oxide nanobelts: synthesis and photocatalytic properties. *Cryst. Eng. Comm.* **12**, 3740 (2010).
27. Sen, U. K. & Mitra, S. Electrochemical activity of $\alpha\text{-}MoO_3$ nano-belts as lithium-ion battery cathode. *RSC Adv.* **2**, 11123 (2012).
28. Wang, S. *et al.* Hydrothermal route to single crystalline $\alpha\text{-}MoO_3$ nanobelts and hierarchical structures. *Solid State Commun.* **136**, 283 (2005).
29. Klinbumrung, A., Thongtem, T. & Thongtem, S. Characterization of orthorhombic $\alpha\text{-}MoO_3$ microplates produced by a microwave plasma process. *J. Nanomater.* **2012** (2012).
30. Wu, F., Deng, N. & Hua, H. Degradation mechanism of azo dye C. I. reactive red 2 by iron powder reduction and photooxidation in aqueous solutions. *Chemosphere* **41**, 1233 (2000).
31. Ovejero, G., Rodríguez, A., Vallet, A. & García, J. Intermediary products in the catalytic wet air oxidation of crystal violet with Ni/MgAlO as catalyst. *Ind. Eng. Chem. Res.* **51**, 11367 (2012).
32. Lin, S. S., Chen, C. L., Chang, D. J. & Chen, C. C. Catalytic wet air oxidation of phenol by various CeO_2 catalysts. *Water Res.* **36**, 3009 (2002).
33. Yao, H. C. & Yao, Y. F. Ceria in automotive exhaust catalysts, I. Oxygen storage. *J. Catal.* **86**, 254 (1984).
34. Chen, H., Sayari, A., Adnot, A. & Larachi, F. Composition–activity effects of Mn–Ce–O composites on phenol catalytic wet oxidation. *Appl. Catal. B: Environ.* **32**, 195 (2001).

Acknowledgments

This work was supported by the Fundamental Research Funds for the Central Universities (TD-JC-2013-3 and BLYJ201402), the Program for New Century Excellent Talents in University (NCET-12-0787), the Beijing Nova Programme (Z131109000413013), the

National Natural Science Foundation of China (51308045), and the Project Sponsored by the Scientific Research Foundation for the Returned Overseas Chinese Scholars, State Education Ministry.

Author contributions

Z.Z. carried out most of the experiments and the analysis of data, and prepared the manuscript. R.Y., Y.G., Y.Z., J.W., L.H., J.G., T.Z., P.L. and Z.G. helped in carrying certain experiments, analysis of certain data, and also provided valuable discussion. Q.W. designed the experiments, analyzed the data, and prepared the manuscript.

Additional information

Supplementary information accompanies this paper at http://www.nature.com/scientificreports

Competing financial interests: The authors declare no competing financial interests.

How to cite this article: Zhang, Z. *et al*. Novel $Na_2Mo_4O_{13}$/α-MoO_3 hybrid material as highly efficient CWAO catalyst for dye degradation at ambient conditions. *Sci. Rep.* **4**, 6797; DOI:10.1038/srep06797 (2014).